

Carbon-doped ZnO: A New Class of Room Temperature Dilute Magnetic Semiconductor

H. Pan,¹ J. B. Yi,² J. Y. Lin,^{1,3} Y. P. Feng,^{1,*} J. Ding,^{2,†} L. H. Van,² and J. H. Yin²

¹*Department of Physics, National University of Singapore,
2 Science Drive 3, Singapore 117542*

²*Department of Materials Science and Engineering,
National University of Singapore, 9 Engineering Drive 1, Singapore 117576*

³*Institute of Chemical and Engineering Sciences,
1 Pesek Road, Jurong Island, Singapore 627833*

(Dated: July 27, 2021)

Abstract

We report magnetism in carbon doped ZnO. Our first-principles calculations based on density functional theory predicted that carbon substitution for oxygen in ZnO results in a magnetic moment of $1.78 \mu_B$ per carbon. The theoretical prediction was confirmed experimentally. C-doped ZnO films deposited by pulsed laser deposition with various carbon concentrations showed ferromagnetism with Curie temperatures higher than 400 K, and the measured magnetic moment based on the content of carbide in the films ($1.5 - 3.0 \mu_B$ per carbon) is in agreement with the theoretical prediction. The magnetism is due to bonding coupling between Zn ions and doped C atoms. Results of magneto-resistance and abnormal Hall effect show that the doped films are *n*-type semiconductors with intrinsic ferromagnetism. The carbon doped ZnO could be a promising room temperature dilute magnetic semiconductor (DMS) and our work demonstrates possibility of producing DMS with non-metal doping.

PACS numbers: 75.50.Pp, 71.55.Gs, 75.50.-y, 85.75.-d

Dilute magnetic semiconductor (DMS) with Curie temperatures (T_c) at or above room temperature is essential for practical spintronics applications. However, synthesis of such materials has been an experimental challenge. DMS is usually produced by doping semiconductors with transition metals (TMs). ZnO and GaN were theoretically predicted to be ideal candidates for room temperature DMS[1]. Even though ferromagnetism has been observed in a number of systems, experimental studies on TM doped ZnO have produced inconsistent results and the mechanism of ferromagnetism in TM doped ZnO remains unclear. It is speculated that TM dopants in ZnO form clusters or secondary phases, which are detrimental to applications of DMS. This promoted search for DMS based on alternative dopants. If non-TM dopants can be incorporated into ZnO and induce magnetism, DMS thus produced would not suffer from problems related to precipitates of dopants since they do not contribute to ferromagnetism. For example, copper doping in ZnO and GaN have been investigated and it has been confirmed experimentally that both Cu doped ZnO and GaN are room temperature DMS. [2, 3, 4, 5, 6, 7, 8] Other DMS obtained by doping with non-TMs, or without doping at all, were also reported, such as Mg doped AlN, Sc-doped ZnO and undoped HfO₂ films. [9, 10, 11, 12]

Ferromagnetism was also reported in a number of carbon systems.[13, 14, 15, 16, 17, 18, 19, 20, 21, 22, 23] Some of these studies have speculated that intrinsic carbon defects could be responsible for the observed magnetic properties. Carbon adatoms on carbon nanotube[24] and carbon substitutional doping in boron nitride nanotube[25] were predicted to induce magnetism in the respective systems. It is therefore of interest to investigate the effect of carbon doping in ZnO and explore the possibility of using carbon as dopant to produce ZnO based DMS. Understanding the mechanism of ferromagnetism in non-metal doped ZnO is useful in exploring new areas of dilute magnetic semiconductors. In this letter, we present our computational and experimental studies on ZnO films doped with carbon and show that the carbon doped ZnO can be a promising DMS.

First-principles calculations based on the density functional theory (DFT) and the local spin density approximation (LSDA) was carried out to investigate carbon doping of ZnO. The plane-wave basis and pseudopotential approach, [26] as implemented in the CASTEP code, [27] was used in our study. In the total energy calculations, the ionic potentials were described by the ultrasoft non-local pseudopotential proposed by Vanderbilt, [28] and the exchange-correlation functional parameterized by Perdew and Zunger [29] was used. The

system was modeled with a periodic supercell of $9.787 \times 9.787 \times 10.411 \text{ \AA}^3$ with 18 formula units of wurzite ZnO, which is sufficient to avoid interaction of C atom with its images in neighboring supercells. An energy cut-off of 310 eV was used for the plane wave expansion of the electronic wave function. Special k points were generated with a $4 \times 4 \times 3$ grid based on Monkhorst-Pack scheme.[30] Good convergence was obtained with these parameters. The total energy was converged to 2.0×10^{-5} eV/atom while the Hellman-Feynman force was smaller than 5.0×10^{-2} eV/ \AA in the optimized structure. We consider three types of carbon doping: carbon interstitial (C_I), carbon substitution at Zn site (C_{Zn}) and carbon substitution at oxygen site (C_O). The calculated lattice constants ($a = 3.25 \text{ \AA}$, $c = 5.20 \text{ \AA}$) for bulk ZnO are in good agreement with the experiment values ($a = 3.25 \text{ \AA}$, $c = 5.21 \text{ \AA}$).[31] The calculated band gap is 1.13 eV within LSDA, which is consistent with the reported results.[32, 33]

Our calculations predicted magnetism in carbon doped ZnO and revealed that it results from carbon substitution for oxygen. Figure 1 shows the calculated local density of states (LDOS) for the carbon dopant and the neighboring Zn atoms. Strong coupling between the carbon s and p orbitals and the s orbital of Zn can be seen. The interaction causes the carbon $2s$ orbital around -9 eV and the carbon $2p$ orbital near 2.3 eV to split. The spin-up bands are fully occupied while the spin-down bands are partially filled, resulting in a magnetic moment of $1.78 \mu_B$ per carbon dopant. The magnetic moment is mainly contributed by the carbon p orbitals ($0.80 \mu_B$), while each of the neighboring Zn atoms and second nearest neighboring oxygen atoms also contribute a small part ($0.1 \mu_B$ and $0.04 \mu_B$, respectively). The estimated formation energy of the C_O defect is 5.3 eV. Similar calculations on carbon substitution for Zn and interstitial carbon showed that they do not result in magnetism.

To verify the theoretical prediction, we prepared C-doped ZnO films using pulsed-laser deposition (PLD). ZnO/ C_x targets with carbon concentrations $x = 0, 0.5, 1, 5$ and 10 were prepared by sintering mixed ZnO (99.9%) and carbon (99.9%) powders in nitrogen atmosphere at 1273 K for 30 min. The base pressure was $< 1 \times 10^{-8}$ torr. The C-doped ZnO films were deposited on sapphire (0001) substrate using a KrF excimer laser operating at 248 nm and a fluence of 1.8 J cm^{-2} . No ferromagnetism was found in the pristine ZnO, carbon powders and sintered ZnO/C targets, as well as the substrates. The films were deposited at 673 K and a vacuum better than 10^{-7} torr in order to ensure epitaxial growth and avoid carbon loss during deposition. The details of the sample preparation procedure was

reported previously.[34] The carbon concentration was estimated based on the secondary ion mass spectrometry (SIMS) analysis with the support from X-ray photoelectron spectroscopy (XPS) and scanning electron microscopy (SEM) examinations. The film thickness was chosen to be 200 nm in order to ensure an accurate estimation of magnetization and to minimize the substrate effect. Three samples with target carbon concentrations of 0, 1 and 5 at%, designated as Sample A, Sample B and Sample C, respectively, were selected for the detailed structural and magnetic study as listed in Table I.

The structures of the ZnO films were characterized by X-ray diffraction (XRD) and SIMS. Our XRD study indicated that both pure and C doped ZnO films show good epitaxy with the sapphire substrate, similar to that of previous study.[34] SIMS analysis showed that Zn and O are uniformly distributed in the C-doped films. Compared with SIMS spectrum of standard reference sample, the average carbon concentration was estimated to be 1 at% and 2.5 at% for the ZnO+1 at%C and ZnO+5 at%C targets, respectively (Table I). It is noted that the carbon concentration in the film is lower than that in the target and thus the carbon loss is severe when the carbon concentration in the target is a higher ($> 3 - 4$ at%).

Carbon can exist in different forms in the grown samples. To verify that carbon is doped into the ZnO films, we carried out further analysis on the samples using XPS and Raman spectroscopy. Two groups of peaks in the C1s binding energy, namely a large peak at 284.6 eV and a few peaks in the energy range of 280 – 284 eV were observed in the XPS analysis. The peak at 284.6 eV can be attributed to “free carbon” (graphite and/or carbon from contamination). Our Raman spectroscopic study confirmed the presence of graphite. New carbon species with C1s binding energy between 280 and 284 eV observed in the C-doped ZnO films suggests presence of carbon atoms in the carbide form,[35] which is an indication of carbon substitution for oxygen and formation of Zn-C bonds in the carbon doped ZnO films.

Magnetic properties of all three samples were investigated. As expected, the pure ZnO film without C doping is non-magnetic, whereas both C doped ZnO films show ferromagnetism at room temperature. A detailed magnetic and electronic investigation was carried out for the two samples - Sample B with a relative low C-doping concentration and Sample C with a high C-doping concentration. The hysteresis loop of Sample B at 300 K, shown in the inset of Fig. 2, clearly shows ferromagnetism. The temperature dependence of magnetization shows a Brillouin type magnetization (Fig. 2). The magnetization at 400 K for

sample B is 3.8 emu/cm^3 , indicating that the Curie temperature of the film is higher than 400 K. The exact Curie temperature could not be directly determined in our experiment due to the limitation of the SQUID system which has a temperature range of $\leq 400 \text{ K}$. However, we fitted the magnetization-temperature curve to the Bloch law,[36] $1 - M_s/M_0 = BT^{3/2}$, where M_s is the magnetization at temperature T , M_0 is the saturation magnetization of the film, and B is a constant. The fitting yielded $B = 5.73 \times 10^{-5} \text{ K}^{2/3}$ and $M_0 = 7.26 \text{ emu/cm}^3$. The Curie temperature of Sample B was thus estimated to be approximately 670 K. Similar fitting shows that Sample C has a higher Curie temperature, approximately 850 K.

We also investigated the dependence of the measured saturation magnetization on carbon concentration in the target, and the results are shown in Fig. 3. The magnetization increases rapidly for low carbon concentrations ($0 - 1 \text{ at}\%$), but becomes saturated when the carbon concentration in the target reaches about $5 \text{ at}\%$. Incidentally, our SIMS and XPS analysis showed that the carbon concentration in the carbide form increases with the target concentration until about $5 \text{ at}\%$ beyond which only the amount of graphite carbon increases and the amount of carbide in the film remains fairly constant, indicating that free carbon do not contribute to the ferromagnetism. By assuming that the XPS peak at 284.6 eV is completely attributed to graphite carbon, and that the carbon due to contamination is negligible, we estimated the magnetic moment per carbon in the ZnO films and obtained values in the range of $2.5 - 3.0 \mu_B$ for Sample B and $1.5 - 2.5 \mu_B$ for Sample C, respectively (Table I). Magnetic moments per carbon of other samples are shown in the inset of Fig. 3. It can be concluded that the magnetic moment in the carbide form is between 1.5 and $3.0 \mu_B$ per carbon for all the C-doped samples, which is in agreement with the theoretical prediction of $1.78 \mu_B$.

As reported previously,[1] magneto-resistance (MR) and abnormal Hall effect (AHE) have been often observed in many DMS's. The AHE is a strong evidence of intrinsic ferromagnetism due to interactions between carriers and spins. In this work, we have studied AHE and MR of carbon-doped ZnO. Figure 4 shows the Hall effect of Sample B at different temperatures. The total Hall effect can be expressed as $\rho_{xy} = R_0B + R_s\mu_0M$, where B is magnetic induction, μ_0 the magnetic permeability, and M the magnetization. The first term above (R_0B) represents the ordinary Hall effect, whereas the second term ($R_s\mu_0M$) denotes the abnormal Hall effect. The normal Hall effect indicates that the films are n -type semiconductor. The hysteresis loop of the Hall effect after the deduction of the normal Hall effect

is shown in the inset. The shape of the Hall effect hysteresis loop is similar to that of the magnetic hysteresis loops measured by SQUID as shown in Fig. 2. The Hall voltage strongly increases with the decreasing of temperature. The abnormal Hall effect also increases with the increasing C-doping concentration, as shown in Table I for Sample C. While Hall mobility decreases with the C-doping concentration, as shown in Table I. In addition, MR up to 0.5% was present in C-doped ZnO. MR was proportional to the measured magnetization.

Ferromagnetism in TM-doped DMS can be due to either double exchange or p - d hybridization mechanism.[37, 38] In the latter, the TM dopant hybridizes strongly with its neighboring anions of the host semiconductors, and the neighboring anions are spin polarized with magnetization in the same order of magnitude as that of the dopant and couple ferromagnetically to the dopant. Other dopants in turn couple to the spin polarized anions in the same way for an energy gain, resulting in an indirect FM coupling among dopants. A similar mechanism can be expected for ferromagnetism in carbon doped ZnO, except that the hybridization here is between the s and p orbitals of the dopant and the s orbitals of the neighboring zinc atoms. As discussed above, the LDOS shown in Fig. 1 indicate a strong hybridization between carbon and its neighboring Zn atoms. This strong hybridization induces finite magnetization on carbon as well as the neighboring Zn atoms. However, further study is necessary to clarify the mechanism for ferromagnetism in carbon doped ZnO.

In conclusion, we demonstrated, both theoretically and experimentally, that carbon can be ferromagnetic when substituting for oxygen in the ZnO environment. Carbon doped ZnO films show an intrinsic n -typed ferromagnetic behavior, with Curie temperatures well above room temperature, which make carbon doped ZnO a promising room temperature DMS and a potentially useful material for spintronics devices. The ferromagnetism originates from the bonding between zinc and doped carbon. Ferromagnetism from carbon doped semiconductors represents a new class of DMS and it opens new possibilities of producing DMS with non-metal doping.

* Electronic address: phyfyp@nus.edu.sg

† Electronic address: msedingj@nus.edu.sg

[1] T. Dietl *et al.*, Science **287**, 1019 (2000).

- [2] R. Q. Wu, *et al.*, Appl. Phys. Lett. **89**, 062505 (2006).
- [3] M. S. Park and B. I. Min, Phys. Rev. B **68**, 224436 (2003).
- [4] C. H. Chien, *et al.*, J. Magn. Magn. Mater. **282**, 275 (2004).
- [5] X. Feng, J. Phys.: Condens. Matter **16**, 4251 (2004).
- [6] L. H. Ye, *et al.*, Phys. Rev. B **73**, 033203 (2006).
- [7] D. B. Buchholz, *et al.*, Appl. Phys. Lett. **87**, 082504 (2005).
- [8] J.-H. Lee, *et al.*, MRS Spring Meeting, 2006.
- [9] R. Q. Wu, *et al.*, Appl. Phys. Lett. **89**, 142501 (2006).
- [10] J. M. D. Coey, Solid State Sci. **7**, 660 (2005).
- [11] M. Venkatesan *et al.*, Phys. Rev. Lett. **93**, 1772061 (2004).
- [12] M. Venkatesan *et al.*, Nature (London) **430**, 630 (2004).
- [13] T. L. Makarova *et al.*, Nature **413**, 716 (2001).
- [14] Y. Kopelevich, *et al.*, J. Low Temp. Phys. **119**, 691 (2000).
- [15] P. Esquinazi, *et al.*, Phys. Rev. B **66**, 024429 (2002).
- [16] X. Wang, *et al.*, J. Phys.: Condens. Matter **14**, 10265 (2002).
- [17] Y. Kopelevich, *et al.*, Phys. Rev. B **68**, 092408 (2003).
- [18] V. Likodimos, *et al.*, Phys. Rev. B **72**, 045436 (2005).
- [19] A. V. Rode, *et al.*, Phys. Rev. B **70**, 054407 (2004).
- [20] K. H. Han, *et al.*, Adv. Mater. **14**, 753 (2002).
- [21] P. Esquinazi, *et al.*, Phys. Rev. Lett. **91**, 227201 (2003).
- [22] P. Esquinazi, *et al.*, Carbon **42**, 1213 (2004).
- [23] S. Talapatra, *et al.*, Phys. Rev. Lett. **95**, 097201 (2005).
- [24] P. O. Lehtinen, *et al.*, Phys. Rev. B **69**, 155422 (2004).
- [25] R. Q. Wu, *et al.*, Appl. Phys. Lett. **86**, 122510 (2005).
- [26] M. C. Payne *et al.*, Rev. Modern. Phys. **64**, 1045 (1992).
- [27] V. Milman *et al.*, J. Quant. Chem. **77**, 895 (2000).
- [28] D. Vanderbilt, Phys. Rev. B **41**, 7892 (1990).
- [29] J. P. Perdew and A. Zunger, Phys. Rev. B **23**, 5048 (1981).
- [30] J. Monkhorst and J. Pack, Phys. Rev. B **23**, 5188 (1976).
- [31] O. Madelung *et al.*, Numerical Data and Functional Relationships in Science and Technology, (Springer-Verlag, Berlin, 1982), Vol. 17.

- [32] A. F. Kohan *et al.*, Phys. Rev. B **62**, 15019 (2000).
- [33] Y. N. Xu and W. Y. Ching, Phys. Rev. B **48**, 4335 (1993).
- [34] L. H. Van *et al.*, J. Alloy & Comp. (in press).
- [35] L. Ramqvist *et al.*, J. Phys. Chem. Solids **30**, 1835 (1969).
- [36] N. Theodoropoulou *et al.*, Phys. Rev. Lett. **89**, 107203 (2002).
- [37] H. Akai, Phys. Rev. Lett. **81**, 3002 (1998).
- [38] K. Sato, *et al.*, J. Phys.: Condens. Matter **16**, S5491 (2004).

TABLE I: The properties of ZnO with and without carbon doping.

| | Sample A | Sample B | Sample C |
|--|----------|------------|------------|
| Carbon concentration of the target (at%) | 0 | 1 | 5 |
| Measured C concentration (at%) | - | ~ 1 | ~ 2.5 |
| Magnetization at 300 K (emg/cm ³) | 0 | 3.8 | 7.1 |
| Magnetization at 5 K (emg/cm ³) | 0 | 7.2 | 10.1 |
| Estimated Curie temperature (K) | 0 | ~ 670 | ~ 850 |
| Moment per C in carbide state | - | 2.0-3.0 | 1.5-2.5 |
| Resistivity ($\Omega\cdot\text{cm}$) | 4 | 0.195 | 0.108 |
| Hall mobility (cm ² /VS) | 94.2 | 22.6 | 14.5 |
| Carrier concentration (10 ¹⁸ /cm ³) | 0.1 | 2.1 | 3.8 |

FIG. 1: Calculated total (top panel) and local density of states for the carbon dopant and a neighboring Zn atom. The Fermi level is indicated by the dashed vertical line.

FIG. 2: $M_s(T)/M_s(5\text{K})$ versus temperature for Sample B and Sample C. The solid lines are curves corresponding to the Bloch law $1 - M_s/M_0 = BT^{3/2}$. The inset shows hysteresis loop taken at 300 K.

FIG. 3: Room temperature saturation magnetization as a function of the target carbon concentration. The inset shows the magnetic moment of carbon in the carbide state in the ZnO films as a function of the target carbon concentration.

FIG. 4: The Hall voltage as a function of magnetic field for Sample B at different temperature. The inset shows the Hall effect curve at 10 K after the normal part is removed.

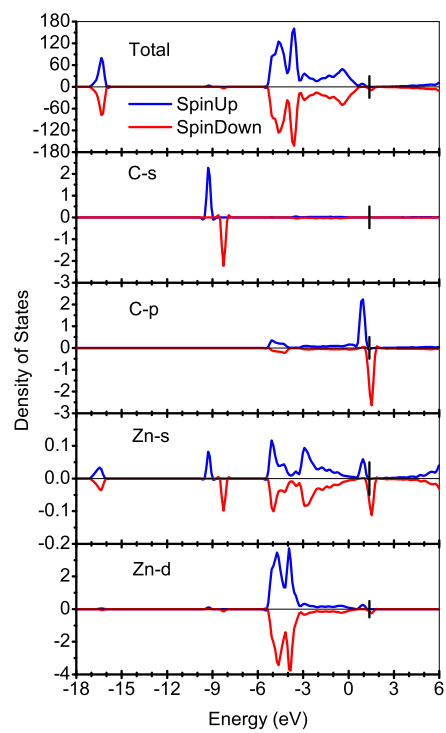


Fig. 1 Pan et al.

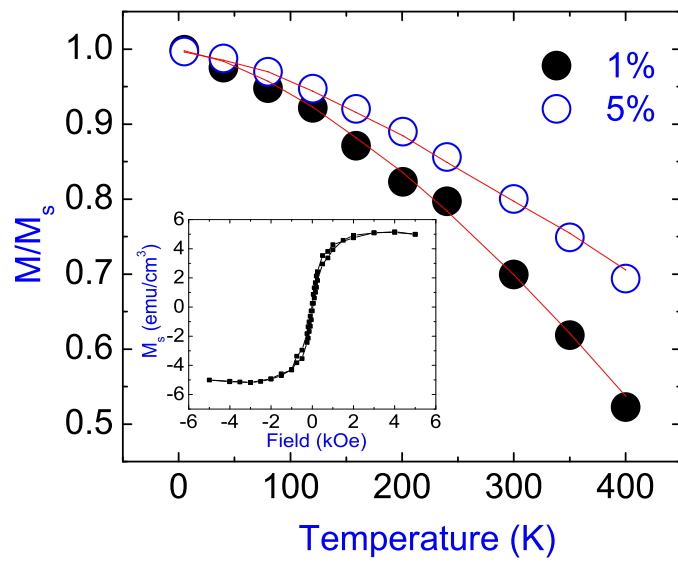


Fig. 2 Pan et al.

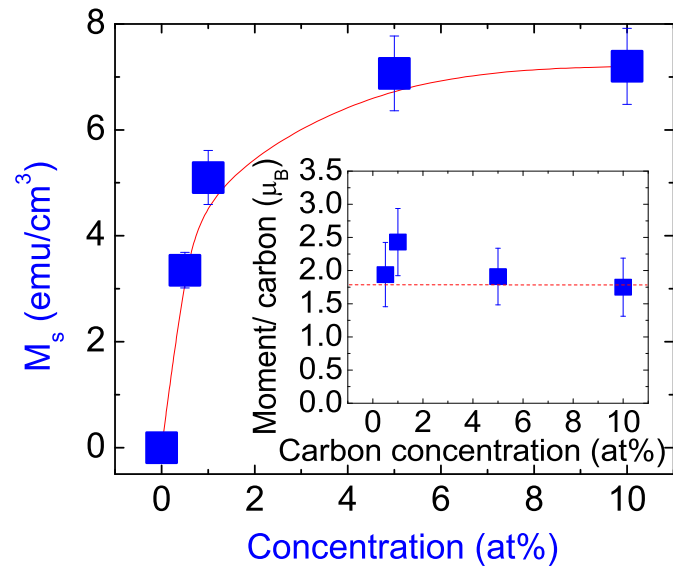


Fig. 3 Pan et al.

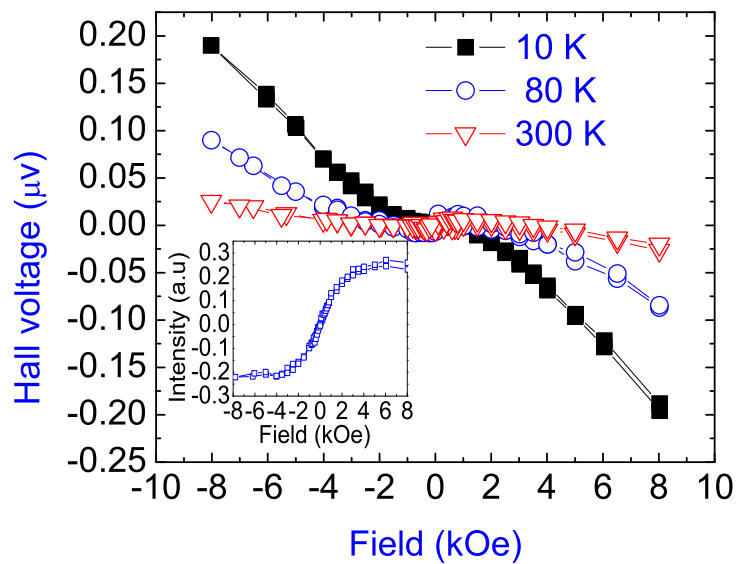


Fig. 4 Pan et al.